



PAPER

Meshfree simulations of ultrasound vector flow imaging using smoothed particle hydrodynamics

RECEIVED
15 June 2018REVISED
18 September 2018ACCEPTED FOR PUBLICATION
24 September 2018PUBLISHED
17 October 2018Shahrokh Shahriari¹ and Damien Garcia^{1,2,3} ¹ Previously, Research Center of the University of Montreal Hospital, Montreal, QC H2X 0A9, Canada² INSA Lyon, Université Claude Bernard Lyon 1, CNRS, Inserm, CREATIS UMR 5220, U1206, Lyon, France³ Author to whom any correspondence should be addressed.E-mail: damien.garcia@inserm.fr and garcia.damien@gmail.com**Keywords:** ultrasound imaging, vector flow imaging, smoothed particle hydrodynamics, blood flow simulations, color Doppler, ultrasound simulationsSupplementary material for this article is available [online](#)**Abstract**

Before embarking on a series of *in vivo* tests, design of ultrasound-flow-imaging modalities are generally more efficient through computational models as multiple configurations can be tested methodically. To that end, simulation models must generate realistic blood flow dynamics and Doppler signals. The current *in silico* ultrasound simulation techniques suffer mainly from uncertainty in providing accurate trajectories of moving ultrasound scatterers. In mesh-based Eulerian methods, numerical truncation errors from the interpolated velocities, both in the time and space dimensions, can accumulate significantly and make the pathlines unreliable. These errors can distort beam-to-beam inter-correlation present in ultrasound flow imaging. It is thus a technical issue to model a correct motion of the scatterers by considering their interaction with boundaries and neighboring scatterers. We hypothesized that *in silico* analysis of emerging ultrasonic imaging modalities can be implemented more accurately with meshfree approaches. We developed an original fluid-ultrasound simulation environment based on a meshfree Lagrangian CFD (computational fluid dynamics) formulation, which allows analysis of ultrasound flow imaging. This simulator combines smoothed particle hydrodynamics (SPH) and Fourier-domain linear acoustics (SIMUS = simulator for ultrasound imaging). With such a particle-based computation, the fluid particles also acted as individual ultrasound scatterers, resulting in a direct and physically sound fluid-ultrasonic coupling. We used the in-house algorithms for fluid and ultrasound simulations to simulate high-frame-rate vector flow imaging. The potential of the particle-based method was tested in 2D simulations of vector Doppler for the intracarotid flow. The Doppler-based velocity fields were compared with those issued from SPH. The numerical evaluations showed that the vector flow fields obtained by vector Doppler components were in good agreement with the original SPH velocities, with relative errors less than 10% and 2% in the cross-beam and axial directions, respectively. Our results showed that SPH-SIMUS coupling enables direct and realistic simulations of ultrasound flow imaging. The proposed coupled algorithm has also the advantage to be 3D compatible and parallelizable.

1. Introduction

Ultrasound imaging is the primary bedside method for evaluating cardiovascular diseases. It can image moving structures in real time, and measure blood velocity or tissue displacement. As an example, carotid examination by ultrasound helps evaluate cardiovascular disease risk in patients with atherosclerotic plaque (Stein *et al* 2008). Of particular interest are Doppler recordings in the internal and external carotids, which allows physicians to identify and assess occlusive carotid plaques. Commonly used clinical Doppler flow imaging modalities are technically limited to scalar measures since they only provide the velocity projection parallel to the direction of

the ultrasound beam. This one-component approach constitutes a particular weak point in Doppler ultrasound given the 3D nature of the cardiovascular flow. Two- and three-component ultrasound techniques have emerged to better decipher blood flow with the purpose of improving diagnosis in patients with cardiovascular disease. Although a number of vector flow methods have been introduced (Jensen *et al* 2016a) and further developed with the expansion of parallel ultrasound (Jensen *et al* 2016b), their clinical additional value has not yet been demonstrated in patients. These methods include blood speckle tracking with or without contrast agent (Trahey *et al* 1987, Fadnes *et al* 2014), Doppler with multiple directions in transmission and/or reception (Fox 1978), transverse oscillations (Jensen and Munk 1998), color-Doppler-based vector flow mapping (Garcia *et al* 2010), and directional beamforming (Jensen and Nikolov 2002). The current research trends show that ultrasound vector flow imaging might become a well-accepted diagnosis tool in the near future (Fadnes *et al* 2015, Assi *et al* 2017, Goddi *et al* 2017, Ricci *et al* 2018). Before its routine bedside utilization in patients, *in vivo* validations are required to ensure that vector flow imaging has a clinical benefit compared with conventional spectral Doppler. Yet several issues need to be considered to mitigate velocity biases in vector flow imaging: numerical robustness, clutter filtering, dealiasing, and regularization, to cite the most important. Before embarking on a series of *in vitro* or *in vivo* tests, design and optimization of vector-flow-imaging modalities are generally more efficient through computational models as multiple configurations can be tested in a relatively short time. To that end, simulation models must generate realistic blood flow dynamics as well as realistic Doppler signals. Early studies that introduced *in silico* ultrasound flow phantoms were based on simple (Poiseuille) flow conditions (Kerr and Hunt 1992b, Jensen and Munk 1997). Individual point scatterers were distributed in the fluid domain to mimic blood components. These scatterers were moved to the next position according to the analytical velocity field. Regarding the study of ultrasound flow imaging in the carotid bifurcation, one can refer to the computational works of Balocco *et al* (2008) and Swillens *et al* (2009). In these studies, the investigators used a commercial computational fluid dynamics (CFD) software (Fluent, Ansys Inc., Canonsburg, US-PA) based on finite volume method to compute pulsatile flows in a carotid bifurcation. The fluid was then seeded with a dense random distribution of acoustic point scatterers. The kinematics of the scatterers were determined from the simulated velocity fields by using successive spatiotemporal interpolations, which returned a Lagrangian description of blood flow and the trajectories of the individual acoustic particles. Radiofrequency RF ultrasound signals were finally obtained using Field II (Jensen 1996), a popular freeware for simulation of medical ultrasound images. Field II allows simulating scattered acoustic fields assuming linear propagation of ultrasound pulses within a collection of weakly backscattering particles (Jensen 1991). The received acoustic fields are estimated by superimposing the individual spherical waves emanating by each point scatterer (Born approximation). Balocco's and Swillens' works present a successful attempt towards computational modeling of realistic physiological color flow imaging. In a similar vein, synthetic ultrasound images of the myocardium can also replicate realistic 3D physiological and pathophysiological conditions for analysis of cardiac strain imaging (Zhou *et al* 2018).

These *in silico* ultrasound simulation techniques, however, suffer mainly from uncertainty in providing accurate trajectories of moving ultrasound scatterers (i.e. their pathlines). When using mesh-based Eulerian methods for time-varying flow fields, pathline computation involves incremental spatial and temporal interpolations. Numerical truncation errors from the interpolated velocities, both in the time and space dimensions, can accumulate significantly and make the pathlines unreliable. These errors can distort beam-to-beam inter-correlation inherently present in ultrasound imaging. It is thus a technical issue to model a physically correct motion of the scatterers considering their interaction with boundaries and neighboring scatterers. Swillens *et al* used a number of numerical tricks to alleviate such problems in weak ultrasound/CFD coupling (Swillens *et al* 2010). Our hypothesis is that *in silico* analysis of emerging ultrasonic imaging modalities can be implemented accurately and efficiently by using particle-based Lagrangian methods. With such meshfree computations, the fluid particles can also act as individual ultrasound scatterers, resulting in a direct and physically sound fluid-ultrasonic coupling. Although it is not the topic of the present manuscript, particle-based approaches have also the advantage to be easily parallelized.

We thus developed a fluid-ultrasound simulation environment based on a meshfree Lagrangian CFD formulation, which allows analysis of ultrasound flow imaging. This simulator combines smoothed particle hydrodynamics (SPH) and linear acoustics. The in-house algorithms for fluid and ultrasound simulations are described in the next section. We then illustrate the potential of the particle-based method by 2D examples of vector Doppler for the intracarotid flow.

2. Methods

2.1. Smoothed particle hydrodynamics (SPH)

Smoothed particle hydrodynamics (SPH) is a Lagrangian numerical method that was originally developed to solve astrophysical problems (Springel 2010). It has then found widespread use in other fields of research, including CFD. In CFD, SPH is used for solving equations of fluid dynamics (mass and momentum conservation,

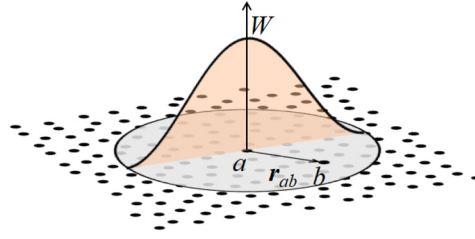


Figure 1. SPH methodology: the intensive physical properties of the particles are smoothed over the set of neighbouring particles enclosed in a compact domain of a smoothing kernel function W .

state equation) by replacing the fluid by a set of discrete particles (Monaghan 2012). Compared to conventional finite or volume element methods, SPH does not require meshing the geometric domain. In SPH, each particle possesses and transports its physical properties (such as mass, pressure and velocity), which are derived by summing the properties of the neighboring particles lying in the domain covered by a compact kernel function (figure 1). Since SPH is a relatively new method, only a few number of simulations for macroscopic blood flow dynamics were reported (Chui and Heng 2010, Yamaguchi *et al* 2010, Shahriari *et al* 2012a, 2012b, Mao *et al* 2016, Caballero *et al* 2017, Shahriari and Kadem 2018). In the present study, we simulated a 2D blood flow in a carotid bifurcation. The moving particles were then directly introduced in an ultrasound simulation software to generate vector Doppler images (see sections 2.2 and 2.3).

We solved the Navier–Stokes equations by using a SPH method to describe blood motion. In this section, we give a short overview of the SPH formulation. We invite readers to refer to key review articles (Monaghan 1992, 2012, Liu and Liu 2010, Price 2012). In SPH, a continuum domain is mapped by a set of particles with no predefined connectivity. Each particle at location \mathbf{r} —defined in a 2D Cartesian coordinate system in our study—has its own intensive physical properties (A), including density, velocity, or pressure. Starting from the equality $A(\mathbf{r}) = \int A(\mathbf{r}') \delta(|\mathbf{r} - \mathbf{r}'|) d\mathbf{r}'$, a smoothed value of A can be given by the weighted integral

$$A(\mathbf{r}) = \int A(\mathbf{r}') W(|\mathbf{r} - \mathbf{r}'|, h) d\mathbf{r}', \quad (1)$$

where W is an even (generally \mathcal{C}^2) weight function whose compact support has a width defined by h (figure 1). W must have the following properties:

$$\int W(|\mathbf{r} - \mathbf{r}'|, h) d\mathbf{r}' = 1, \quad \text{and} \quad \lim_{h \rightarrow 0} W(|\mathbf{r} - \mathbf{r}'|, h) = \delta(|\mathbf{r} - \mathbf{r}'|). \quad (2)$$

In SPH-based CFD, the fluid is divided into a set of particles to discretize the integral interpolant (1). Substituting the elementary volume $d\mathbf{r}'$ with a ratio of mass to density yields, for a particle labeled as ‘ a ’,

$$A_a \equiv A(\mathbf{r}_a) = \sum_b \left\{ A_b \frac{m_b}{\rho_b} W_{ab} \right\}, \quad \text{with} \quad W_{ab} \equiv W(|\mathbf{r}_a - \mathbf{r}_b|, h) \quad (3)$$

where m_b and ρ_b stand for the mass and density of particle ‘ b ’. In our study, we chose $m_b = m, \forall b$ and a quartic spline kernel W , as in a previous study (Shahriari *et al* 2013). Since W is even and compactly supported, it can be shown that the discretized gradient for particle ‘ a ’ is given by

$$\nabla_a A = \sum_b \left\{ A_b \frac{m_b}{\rho_b} \nabla_a W_{ab} \right\}, \quad (4)$$

where ∇_a represents the gradient associated to particle ‘ a ’, i.e. at location \mathbf{r}_a . Of important note, higher accuracy is obtained by considering density in the gradient operator, then defined as follows

$$\nabla A = \frac{1}{\rho} (\nabla(\rho A) - A \nabla \rho) \quad (5a)$$

or

$$\nabla A = \rho \nabla \left(\frac{A}{\rho} \right) + \frac{A}{\rho} \nabla \rho. \quad (5b)$$

The use of one or the other depends on whether the parameter is symmetrical. Details can be found in section 2.4 in Liu and Liu (2010). It follows that (4) becomes

$$\nabla_a A = \frac{1}{\rho_a} \sum_b \{ m_b (A_b - A_a) \nabla_a W_{ab} \} \quad (6a)$$

or

$$\nabla_a A = \rho_a \sum_b \left\{ m_b \left(\frac{A_b}{\rho_b^2} + \frac{A_a}{\rho_a^2} \right) \nabla_a W_{ab} \right\}. \quad (6b)$$

The principle of mass conservation relates density and velocity \mathbf{u} . It reads $D_t \rho = -\rho \nabla \cdot \mathbf{u}$, with D_t representing the material (Lagrangian) derivative. Using (6a), conservation of mass leads to

$$D_t \rho_a = \sum_b \left\{ m_b (\mathbf{u}_a - \mathbf{u}_b) \cdot \nabla_a W_{ab} \right\}. \quad (7)$$

In grid-based methods, fluid is generally assumed to be incompressible when the speed of sound is large compared with bulk fluid speeds. In SPH, however, fluid pressure (p) is related to density through a quasi-incompressible equation of state. In an isentropic fluid flow, the speed of sound is given by $c^2 = \partial p / \partial \rho$. We thus used the following equation of state

$$p_a = c^2 (\rho_a - \rho_0), \quad (8)$$

with $\rho_0 = 1000 \text{ kg m}^{-3}$. Although the speed of sound in blood is around 1500 m s^{-1} , it can be considerably reduced in SPH simulations to avoid small computational time steps as long as density fluctuations are within an acceptable range to maintain quasi-incompressibility (Morris *et al* 1997).

In the absence of body accelerations, the quasi-incompressible Navier–Stokes equation for a Newtonian fluid is

$$D_t \mathbf{u} = -\frac{1}{\rho} \nabla p + \frac{\mu}{\rho} \Delta \mathbf{u}, \quad (9)$$

with μ being the dynamic viscosity. Using (6b), the SPH formulation of the internal pressure source is

$$-\frac{1}{\rho_a} \nabla_a p \xrightarrow{(6b)} -\sum_b \left\{ m_b \left(\frac{p_b}{\rho_b^2} + \frac{p_a}{\rho_a^2} \right) \nabla_a W_{ab} \right\}. \quad (10)$$

It is possible to derive an SPH approximation for the viscous diffusion term (i.e. the 2nd term of the right-hand side in (9)) by using the second derivative of the smoothing kernel, in a similar manner to equation (4). For some reasons not explained here, this generally leads to physically incorrect effects. Several types of viscosity term have thus been introduced; see e.g. (Price 2012, Shahriari and Kadem 2018) for a number of examples. In our study, we used an original, physically and numerically sound form. It is noticeable that the fundamental spaces for SPH are open balls whose radius ($\equiv \kappa h$, with κ a kernel-dependent scalar) is defined by the compact support of W . Using Taylor's theorem, the Laplacian of a function can be linked to the mean value of this function on a ball (see equation (13) in Ovall (2016)). In two dimensions, for a ball (disk) of radius κh centered in a particle 'a', it gives

$$\bar{A} = A_a + \frac{\kappa^2 h^2}{8} \Delta_a A + \mathcal{O}(h^3), \quad (11)$$

where \bar{A} is the mean value of A on the disk, and $\Delta_a A$ is the Laplacian of A at location \mathbf{r}_a . Using a weighted arithmetic mean, an SPH viscous form (in 2D) can be given by

$$\frac{\mu}{\rho_a} \Delta_a \mathbf{u} \xrightarrow{(11)} \frac{8}{\kappa^2 h^2} \frac{\mu}{\rho_a} \frac{\sum_b \left\{ (\mathbf{u}_b - \mathbf{u}_a) \frac{m_b}{\rho_b} W_{ab} \right\}}{\sum_b \left\{ \frac{m_b}{\rho_b} W_{ab} \right\}}. \quad (12)$$

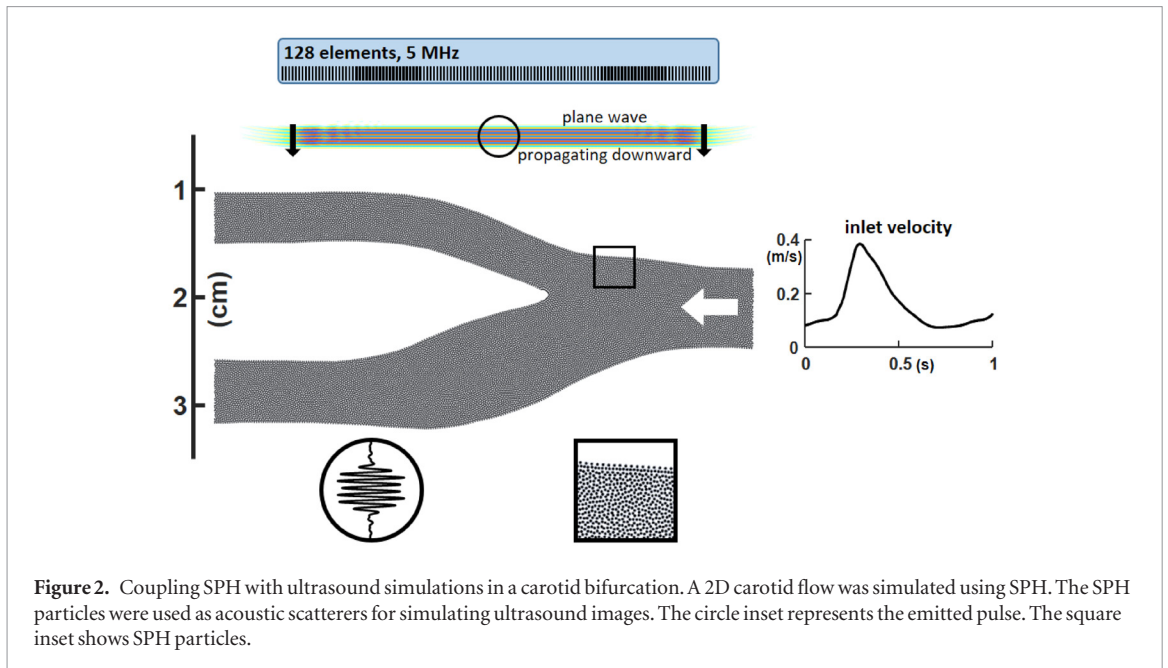
Replacing the two terms of the right-hand side in (9) by their SPH counterparts finally yields

$$D_t \mathbf{u}_a = -\sum_b \left\{ m_b \left(\frac{p_b}{\rho_b^2} + \frac{p_a}{\rho_a^2} \right) \nabla_a W_{ab} \right\} + \frac{8}{\kappa^2 h^2} \frac{\mu}{\rho_a} \frac{\sum_b \left\{ (\mathbf{u}_b - \mathbf{u}_a) \frac{m_b}{\rho_b} W_{ab} \right\}}{\sum_b \left\{ \frac{m_b}{\rho_b} W_{ab} \right\}}. \quad (13)$$

We numerically solved the system composed of equations (7), (8) and (13) to simulate a pulsatile flow in a 2D carotid bifurcation.

2.2. SPH in a 2D carotid artery model

A 2D pulsatile flow phantom was constructed based on a model of healthy carotid bifurcation (figure 2). We assumed a Newtonian blood fluid (i.e. with constant viscosity). The geometry and inlet velocity were inspired from magnetic resonance measurements published in Zhao *et al* (2003). The diameter of the common, internal and external carotids were 8, 5.55 and 4.65 mm, respectively. A fully developed velocity waveform was imposed at the inlet of the common carotid (figure 2), with a peak at 0.39 m s^{-1} , a mean Reynolds number of 375, and a period of 830 ms. Similar velocity waveforms were imposed at the outlet boundaries (internal and external outlets), with respective ratios of 54% and 46% with respect to inlet flow rate. A total of ~ 26000 SPH particles



were initially distributed on a square lattice with spacing of 0.15 mm. The number of SPH particles were chosen so that the density of random scatterers ensured proper echo envelope statistics (Destremes and Cloutier 2010). For this reason, particle density was larger than that used in our previous validation study on oscillating flows (Shahriari *et al* 2013), thus increasing computational load. In the present study, we did not investigate the effect of particle number on numerical convergence of SPH since flow high-accuracy was not a critical issue. Fixed virtual particles were allocated on (type I) and outside (type II) solid boundary walls (see section 5.1 in Liu and Liu (2010) for details). Type I particles had a null velocity with same pressure and density as their closest fluid particles. Extrapolated velocities were assigned to type II particles to get no-slip and pressure Neumann boundary conditions. The implementation of the inflow, outflow and wall-boundary conditions and the problem of reseeding were described in detail in a previous paper (Shahriari *et al* 2012a). In particular, we used a numerical trick involving virtual inflow and outflow reservoirs, as explained in Shahriari *et al* (2012a). A second order predictor-corrector method was used to solve the differential equations (7) and (13). The maximal time increment was determined by the Courant–Friedrichs–Levy condition (Courant *et al* 1967). A total of 8×32 fixed time instants were also imposed at $(0.1, 0.2, \dots 0.8 \text{ s}) + (0.1, 0.2, \dots 3.2 \text{ ms})$. They were used to simulate 8 vector Doppler fields, each one of them created from a packet size of 32 at a PRF of 10 kHz (see section 2.4 for details). These additional time instants increased the time step (at the expense of computational cost) but did not jeopardize numerical stability. The velocity profiles generated by the 2D SPH carotid model were qualitatively compared with those measured by magnetic resonance and reported in Zhao *et al* (2003) to verify their physiological reliability.

2.3. SIMUS: simulation of ultrasound imaging

Using the SPH fluid particles, we simulated color Doppler images by using an in-house software written in Matlab language (we called it SIMUS). SIMUS simulates backscattered ultrasound signals for a uniform linear array (ULA) in a 2D domain. This ultrasound-imaging simulator is based on the linear wave equation written in the frequency domain for a uniform medium (constant speed of sound). The acoustic pressure field generated by the ULA in the far field of each element—not necessarily in the far field of the array—can be written as (see equation (4.10) p 76 in Schmerr (2015a))

$$P(x, z, \omega, t) = \rho c v_0(\omega) \sum_{n=1}^N W_n e^{i\omega \Delta \tau_n} \left[\sqrt{\frac{2}{i\pi}} k b D_b(\theta_n, k) \frac{e^{ikr_n}}{\sqrt{kr_n}} \right] e^{-i\omega t}, \quad (14)$$

where $i = \sqrt{-1}$, t is time, ω is the angular frequency, ρ is the medium density, c is the speed of sound and $k = \omega/c$ is the wavenumber. In this equation, it is assumed that the N individual elements of the ULA act as pistons whose normal velocity in the frequency domain is $v_0(\omega)$. The location (x, z) is defined in the Cartesian coordinate system related to the ULA (figure 2). In this coordinate system, the centroid location of the n th element is given by $x_n = (2n - 1 - N) / (2p)$ and $z_n = 0$, with p being the pitch of the linear array. The distances r_n are $r_n = \sqrt{(x - x_n)^2 + z^2}$; the angles θ_n are given by $\sin(\theta_n) = (x - x_n) / r_n$. The weights W_n applied to the N elements represent the apodization values. Because no apodization was considered in our study, $W_n = 1, \forall n$.

The frequency-dependent function $D_b(\theta, k)$ is the directivity function of an individual element of width $2b$. It was assumed that the transducer elements were surrounded by a soft baffle (Selfridge *et al* 1980), so that

$$D_b(\theta, k) = \cos \theta \frac{\sin(kb \sin \theta)}{kb \sin \theta}. \quad (15)$$

The parameters $\Delta\tau_n$ represent the transmit delay laws. Since we simulated transmissions of non-steered plane waves, $\Delta\tau_n = 0, \forall n$, in our study. Equation (14) thus reduced to

$$P(x, z, \omega, t) = \underbrace{(\rho c \sqrt{kb} v_0(\omega))}_{\propto P_{Tx}(\omega)} \sum_{n=1}^N \left[\sqrt{\frac{2}{i\pi}} D_b(\theta_n, k) \frac{e^{ikr_n}}{\sqrt{r_n/b}} \right] e^{-i\omega t}. \quad (16)$$

Note that $\sqrt{r_n}$ and \sqrt{k} appear in these equations (instead of r_n and k in 3D) since we considered a 2D model. The first term in brackets (dimensionally homogeneous to a pressure) represents the spectrum of the transmit pulse (up to a constant multiplier). In SIMUS, the acoustic scatterers (i.e. the 26 000 SPH particles in this study) become individual monopole point sources when the incident wave reaches them. It is also assumed that the scatterers do not acoustically interact with each other (single scattering). The acoustic pressure measured by the single elements of the ULA thus results from the sum of the M individual backscattered cylindrical (or spherical in 3D) waves. The acoustic pressure measured by the q th element of the ULA is thus given by (up to a constant multiplier):

$$P_{Tx}(\omega) \sum_{m=1}^M \left[\text{BSC}_m \left(\sum_{n=1}^N \left[D_b(\theta_{nm}, k) \frac{e^{ikr_{nm}}}{\sqrt{r_{nm}/b}} \right] \right) D_b(\theta_{qm}, k) \frac{e^{ikr_{qm}}}{\sqrt{r_{qm}/b}} \right] e^{-i\omega t}, \quad (17)$$

where $r_{ij} = \sqrt{(x_i - x_j)^2 + z_j^2}$ and $\sin(\theta_{ij}) = (x_i - x_j) / r_{ij}$. The parameter BSC_m represents the backscattering coefficient of the m^{th} particle. Although blood is governed by Rayleigh scattering in medical imaging ultrasound (Mo and Cobbold 1986), the BSC_m were assumed constant (i.e. independent of frequency and incidence angle). To mimic homogeneous tissues, we considered that the backscattering coefficients follow a Gaussian distribution (Jensen and Munk 1997):

$$\text{BSC}_m \sim \sigma_m \mathcal{N}(0, 1), \quad (18)$$

where the standard deviation σ_m adjusts the backscattering strength. Note that absorption can be directly integrated in the ultrasound model by using a complex wavenumber $k' = k + i\alpha$, with α standing for the absorption coefficient. In this study, however, absorption was neglected.

2.4. Simulation of color Doppler and vector Doppler

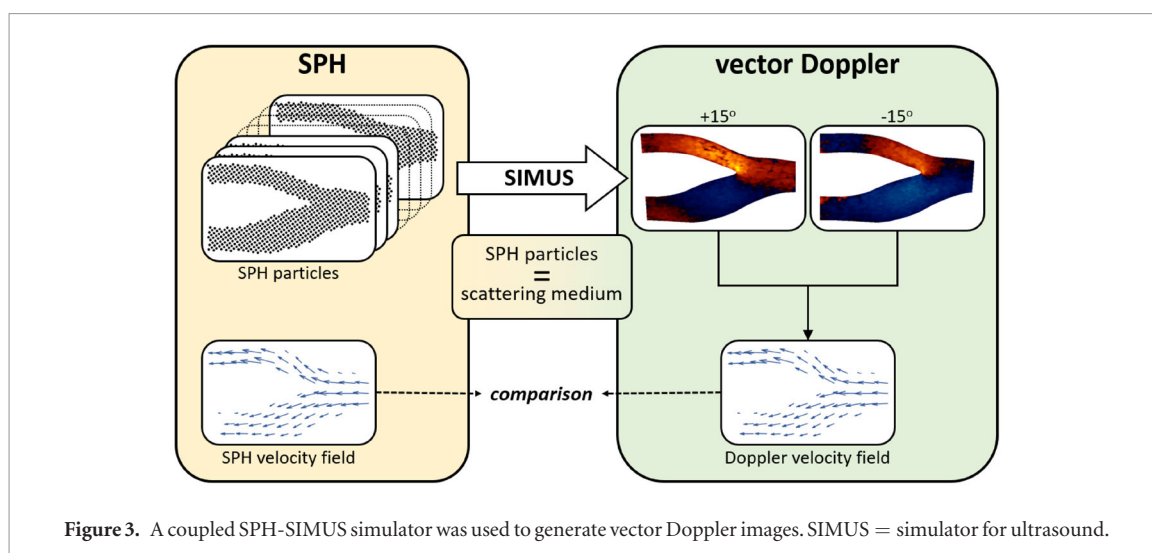
We simulated non-steered plane waves (i.e. $\Delta\tau_n = 0$ in (14)) transmitted at a pulse repetition frequency (PRF) of 10 kHz by a 5 MHz linear array (128 elements, pitch = 0.30 mm, kerf = 35 μm). Each pulse was a windowed sine of width 6 wavelengths ($6/5 \cdot 10^6 = 1.2 \mu\text{s}$, figure 2). The RF (radio-frequency) signals received by the 128 elements were assumed to be proportional to the received acoustic pressures (equation (17)). The RF signals were demodulated to yield I/Q signals, which were then migrated onto a regular grid using a diffraction summation (delay-and-sum). Two receive subapertures were used to generate the vector flow images (Papadofrangakis *et al* 1981, Tanter *et al* 2002), with an f -number of 3 (Madiena *et al* 2018). The two receive beam angles were $\varphi_{1,2} = \mp 15^\circ$. Eight pairs of color Doppler velocities (at respective times 0.1, 0.2, ... 0.8 s) were estimated from the beamformed I/Q components using a standard slow-time autocorrelator of lag 1 and a packet size of 32. In mathematical terms, if $v_{D\{j\}}$ stands for Doppler velocities related to receive beam angle $\#j$ (with $j = 1, 2$), the Doppler components were given by:

$$v_{D\{j\}} = -\frac{c \text{ PRF}}{4\pi f_0} \text{Im} \left\{ \ln(\mathcal{R}_1\{j\}) \right\}, \quad (19)$$

where f_0 is the center frequency (5 MHz), PRF is the PRF and \mathcal{R}_1 is the lag-1 slow-time autocorrelation of the I/Q signals. The operators Im and ln represent the imaginary part and natural logarithm, respectively. Vector Doppler fields were generated from each pair through trigonometric manipulations (Yiu *et al* 2014). From equation (4) in Jensen *et al* (2016a), our configuration (i.e. non-steered transmits, two receive angles $\varphi_{\{j=1,2\}} = (-1)^j \times 15^\circ$) led to:

$$\begin{cases} v_x = \frac{v_{D\{2\}} - v_{D\{1\}}}{\sin|\varphi|} \\ v_z = \frac{v_{D\{2\}} + v_{D\{1\}}}{1 + \cos|\varphi|} \end{cases}. \quad (20)$$

These velocity vector fields were finally smoothed using a robust and unsupervised regularizer (Garcia 2010). This regularizer has been validated for velocity vector fields in the context of particle image velocimetry (Garcia 2011).



The Doppler-derived velocity vectors were compared with the ground-truth SPH vector fields by calculating the errors on the x - and z -components relative to the maximal speed. Figures 2 and 3 provide an overview of the simulation protocol.

3. Results

3.1. Carotid artery model

Figure 4 qualitatively compares transient velocity magnitudes returned by the 2D SPH model with *in vivo* magnetic resonance measurements reported in Zhao *et al* (2003). The results illustrate an acceptable agreement and show that the SPH-derived flow fields were respectably physiological for analyzing the coupled SPH-SIMUS simulator. Differences are mostly justified by the fact that our results were 2D, whereas the reference data were extracted from 3D magnetic resonance imaging (Zhao *et al* 2003).

3.2. Color Doppler and vector Doppler

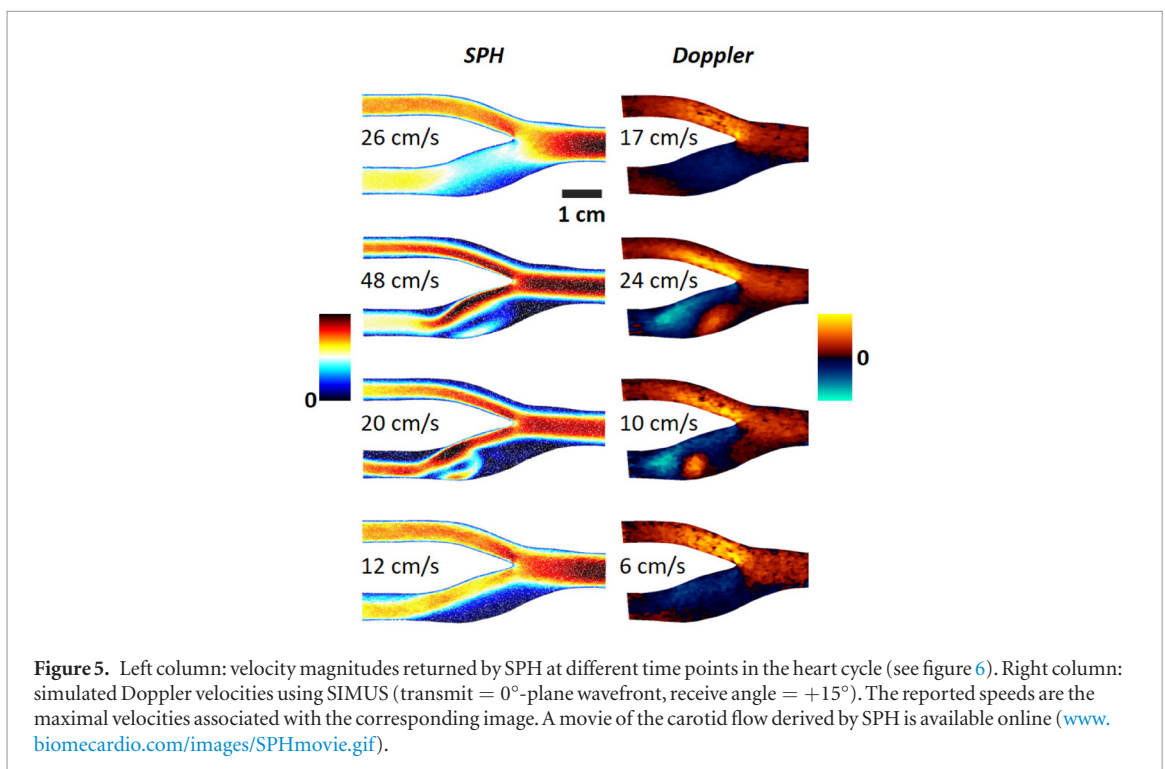
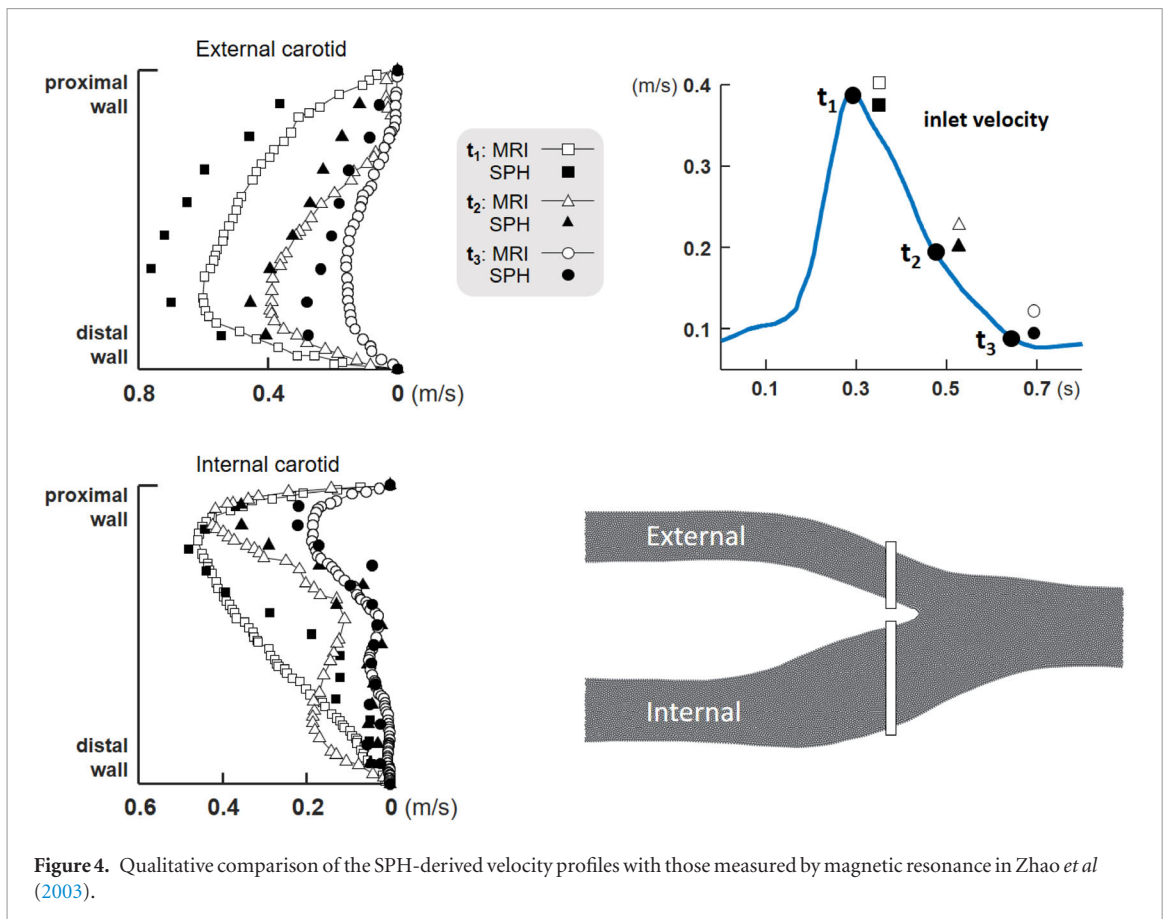
The direct coupling SPH-particles/acoustic-scatterers in the SPH-SIMUS simulator provided realistic color Doppler (figure 5). Figure 5 reports a series of color Doppler images with a receive angle of $+15^\circ$. Combining them with the color Doppler images obtained at -15° yielded vector Doppler images illustrated in figure 6 (left column). There was a very good concordance with the actual SPH-velocity field (right column). The distribution of the relative errors (vector Doppler versus SPH) throughout one cardiac cycle is reported in figure 6. The relative errors of the z -components (x -components) were in the $\pm 2\%$ ($\pm 10\%$) range for 75% of the data (figure 7).

4. Discussion

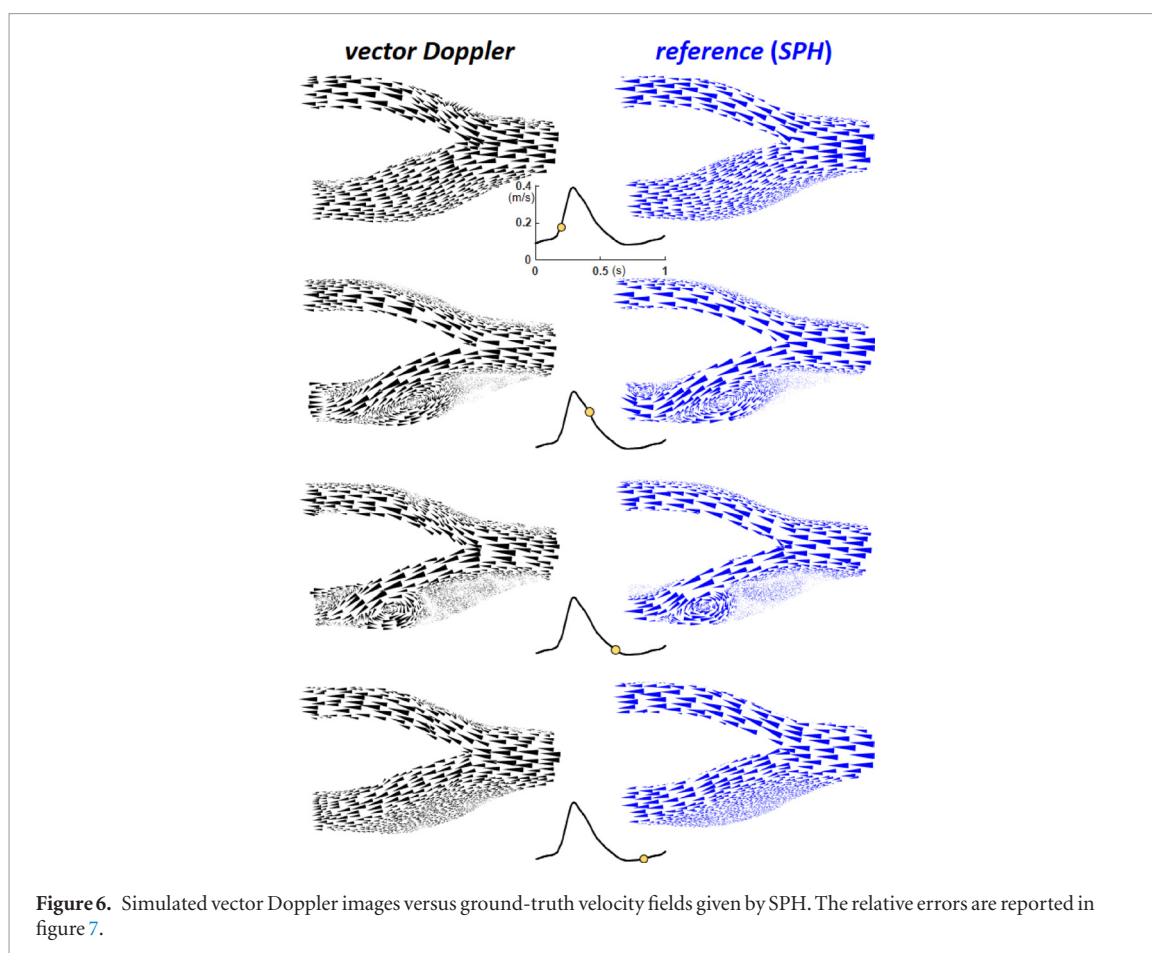
4.1. SPH for ultrasound flow imaging

As introduced in section 2.1, SPH is a Lagrangian numerical method that has found extensive applications in CFD. Since it is meshfree, a specific interest has been demonstrated in free surface and multiphase flows, as well as in flows around complex fixed or moving bodies. SPH has also been shown of high significance for fluid-structure interaction (FSI) in the presence of highly deformable structures. SPH algorithms, in their basic form, are easy to program and easy to parallelize. Compared with mesh-based methods, however, one difficulty encountered in SPH might be the implementation of inlets, outlets, and pressure boundary conditions, especially if high accuracy is required. Wall management also requires special attention. In this study, we investigated SPH in the context of color flow imaging by ultrasound. Reaching high velocity accuracy was thus not necessary since the problem did not involve large-scale differences: e.g. it was not our goal to resolve small-scale turbulence and mixing present in diverging blood flows (Pibarot *et al* 2013), whose fine structures cannot be grasped with standard clinical transducers. Our objective was to introduce an all-in-one simulation tool able to generate realistic color Doppler images.

To simulate clinical ultrasound flow imaging, a dense set of buoyant-free point scatterers must seed a flowing fluid to mimic blood backscattering. SPH was thus a natural option for CFD as the SPH fluid particles also acted as acoustic sources in the ultrasound simulator SIMUS. This strategy allowed a direct coupling between fluid and acoustic simulations. As deeply discussed in Swillens *et al* (2009), this fluid/acoustic coupling requires special numerical considerations with Eulerian mesh-based CFD methods. In particular, the distribution of the scatterers must be restored at different time intervals to prevent spurious particle dilution or aggregation and preserve



beam-to-beam ultrasound correlation. In contrast to standard CFD techniques (typically finite volumes, finite elements, or finite differences) that involve mesh generation, SPH offers direct pairing between fluid and acoustic particles. We had no need to calculate trajectories from Eulerian velocity fields, which ensured numerical stability and robustness. Except for some numerical drawbacks discussed above, another key benefit of SPH is its relative ease of implementation. In this study, we implemented an in-house SPH code whose accuracy had been validated in three different test cases (Shahriari *et al* 2012a). Overall, our results thus showed that SPH is particularly appropriate for simulating cardiovascular blood flows in the specific context of ultrasound imaging.



4.2. Ultrasound simulation using SIMUS

A number of ultrasound-related free software has been introduced in the literature for a variety of applications, for example (Jensen and Munk 1997, Treeby and Cox 2010, Varray *et al* 2013). Among these tools for ultrasound acoustic modelling, Field II (Jensen 1996) is a popular simulator based on the linear spatial impulse response of an array of pistons embedded in an infinite baffle (Stepanishen 1971). In contrast to other software, Field II allows simulations of ultrasound color Doppler images. Inspired from seminal works (Foster *et al* 1983, Kerr and Hunt 1992a, 1992b), it considers stationary or moving media of randomly located point scatterers. The backscattered radiofrequency RF signals are calculated by summing the individual responses of each scatterer. Our in-house SIMUS software is based on the same principles except that it works in the frequency domain. Frequency-domain modelling of ultrasound B-mode images with ULAs has been proposed by Li and Zagzebski (1999). Frequency-domain models have some advantages over time-domain models. (1) Frequency-dependent attenuation can be integrated naturally. (2) The same applies to frequency-dependent directivity of the elements and to (3) Rayleigh scattering. (4) High temporal sampling rates are needed to guarantee accuracy in time-domain models, which increases computational load. (5) Long transmit pulses, such as chirp waveforms, also increase computational load in time-domain models. A far-field approximation is used in SIMUS to simplify the algorithm. To get accurate results in the near-field of the array, the transducer elements can be split into small segments so that the far-field approximation given by equation (14) remains valid near the transducer. This model, which is called the ‘multiple line source array beam model’ by Schmerr (2015b), forms the foundation of SIMUS. Of important note, SIMUS is based on linear acoustics. Non-linear responses such as those observed in contrast harmonic imaging cannot be simulated. Specific software, as the one proposed by Varray *et al* (2013), is required to simulate nonlinear components of the ultrasound wave. Since we focused on the SPH-acoustics coupling in the present work, a comprehensive description of SIMUS is beyond the scope of this article. Comprehensive theoretical and numerical details on the ultrasound model will be the subject of a future paper.

4.3. Limitations and perspectives

Because there is no formal color-Doppler ground-truth, it was not possible to quantify accuracy and precision of the simulated color Doppler images. Although it may sound subjective, we however obtained very realistic color Doppler images. By ‘realistic’, we mean that the simulated color Doppler images resembled those obtained in a clinical context (figure 5). More realistic ultrasound images should also contain moving walls to incorporate

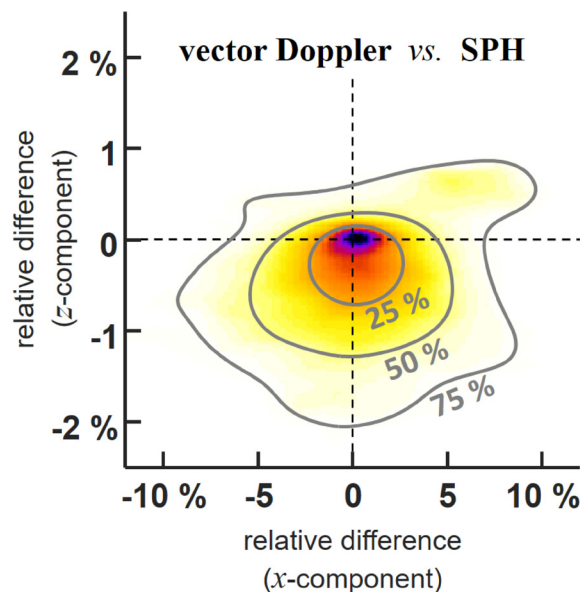


Figure 7. Distribution of the relative errors in simulated vector Doppler as compared with SPH.

clutter and side-lobe artifacts. In addition, to simplify matters, the simulations described in this study were all 2D. Although they demonstrate the advantages of SPH for modelling ultrasound color Doppler, our results were not fully physiological since they did not reflect the 3D nature of blood flow. Extending the SPH and SIMUS tools to 3D will not lead to algorithm and numerical issues since both models are well suited for 3D applications. The major obstacle will rise from the number of fluid particles/acoustic scatterers (hundreds of thousands) that will be necessary to provide accurate SPH flows and realistic 3D color Doppler. SPH and SIMUS, however, are easily parallelizable, which will help to reduce computational time. Indeed, SPH fluid particles can be analyzed independently as long as their respective compact neighborhood (figure 1) do not overlap. In SIMUS, the scatterers can also be studied individually since the acoustic model is based on weak (single) scattering. The SIMUS code that we used in this study was executed in parallel on several Matlab workers. Generalization to 3D parallel computing will be thus the next stage. It was also assumed that the wall was rigid. Although FSI can be efficiently implemented by SPH (Antoci *et al* 2007), we did not consider FSI for the sake of simplicity. A mesh-based simulation environment for vascular ultrasound flow imaging including FSI was first proposed by Swillens *et al* (2010). SPH could be a promising alternative since it can manage large structure displacements in a more efficient manner than mesh-based approaches. A topic of interest would be the simulation of the large-scale vortical flow that occurs in the left ventricle downstream from the mitral valve (Mao *et al* 2017). It is known that this vortex may reflect the diastolic function (i.e. the filling capacity of the heart) (Arvidsson *et al* 2016). Coupled SPH-acoustics simulations could help to (1) better understand how the vortex properties relate to myocardial relaxation and mitral valve dynamics (Chnafa *et al* 2014, Mao *et al* 2017), and (2) improve intraventricular vortex characterization by ultrasound imaging (Mehregan *et al* 2014, Assi *et al* 2017).

5. Conclusion

We have introduced a mesh-free coupled fluid-ultrasound simulation tool based on SPH and linear phased array acoustics. In this Lagrangian approach, the fluid particles also act as acoustic scatterers, which ensures strong multi-physics coupling while inherently preserving beam-to-beam ultrasound correlation. Mesh-free fluid-ultrasound simulations will be beneficial for improving/exploring current/new methods and algorithms for ultrasound flow imaging.

Acknowledgments

This work was supported in part by the Fonds de recherche du Québec—Nature et technologies (FRQNT) through a postdoctoral fellowship (#168745) granted to the first author. Dr Garcia held a research scholarship award from the Fonds de Recherche en Santé du Québec (FRSQ) when he started this project. He presently has a starting research grant from INSERM (French National Institute of Health and Medical Research).

ORCID iDs

Damien Garcia  <https://orcid.org/0000-0002-8552-1475>

References

- Antoci C, Gallati M and Sibilla S 2007 Numerical simulation of fluid–structure interaction by SPH *Comput. Struct.* **85** 879–90
- Arvidsson P M, Kovács S J, Töger J, Borgquist R, Heiberg E, Carlsson M and Arheden H 2016 Vortex ring behavior provides the epigenetic blueprint for the human heart *Sci. Rep.* **6** 22021
- Assi K C, Gay E, Chnafa C, Mendez S, Nicoud F, Abascal J F P J, Lantelme P, Tournoux F and Garcia D 2017 Intraventricular vector flow mapping—a Doppler-based regularized problem with automatic model selection *Phys. Med. Biol.* **62** 7131–47
- Balocco S, Basset O, Azencot J, Tortoli P and Cachard C 2008 3D dynamic model of healthy and pathologic arteries for ultrasound technique evaluation *Med. Phys.* **35** 5440–50
- Caballero A, Mao W, Liang L, Oshinski J, Primiano C, McKay R, Kodali S and Sun W 2017 Modeling left ventricular blood flow using smoothed particle hydrodynamics *Cardiovasc. Eng. Technol.* **8** 465–79
- Chnafa C, Mendez S and Nicoud F 2014 Image-based large-eddy simulation in a realistic left heart *Comput. Fluids* **94** 173–87
- Chui Y-P and Heng P-A 2010 A meshless rheological model for blood–vessel interaction in endovascular simulation *Prog. Biophys. Mol. Biol.* **103** 252–61
- Courant R, Friedrichs K and Lewy H 1967 On the partial difference equations of mathematical physics *IBM J. Res. Dev.* **11** 215–34
- Destremes F and Cloutier G 2010 A critical review and uniformized representation of statistical distributions modeling the ultrasound echo envelope *Ultrasound Med. Biol.* **36** 1037–51
- Fadnes S, Ekroll I K, Nyrnes S A, Torp H and Lovstakken L 2015 Robust angle-independent blood velocity estimation based on dual-angle plane wave imaging *IEEE Trans. Ultrason. Ferroelectr. Freq. Control* **62** 1757–67
- Fadnes S, Nyrnes S A, Torp H and Lovstakken L 2014 Shunt flow evaluation in congenital heart disease based on two-dimensional speckle tracking *Ultrasound Med. Biol.* **40** 2379–91
- Foster D R, Arditi M, Foster F S, Patterson M S and Hunt J W 1983 Computer simulations of speckle in B-scan images *Ultrason. Imaging* **5** 308–30
- Fox M D 1978 Multiple crossed-beam ultrasound Doppler velocimetry *IEEE Trans. Sonics Ultrason.* **25** 281–6
- Garcia D 2010 Robust smoothing of gridded data in one and higher dimensions with missing values *Comput. Stat. Data Anal.* **54** 1167–78
- Garcia D 2011 A fast all-in-one method for automated post-processing of PIV data *Exp. Fluids* **50** 1247–59
- Garcia D *et al* 2010 Two-dimensional intraventricular flow mapping by digital processing conventional color-Doppler echocardiography images *IEEE Trans. Med. Imaging* **29** 1701–13
- Goddi A, Bortolotto C, Fiorina I, Raciti M V, Fanizza M, Turpini E, Boffelli G and Calliada F 2017 High-frame rate vector flow imaging of the carotid bifurcation *Insights Imaging* **8** 319–28
- Jensen J A 1991 A model for the propagation and scattering of ultrasound in tissue *J. Acoust. Soc. Am.* **89** 182–90
- Jensen J A 1996 FIELD: a program for simulating ultrasound systems *10th Nordic Baltic Conf. on Biomedical Imaging, Vol. 4, Supplement 1, Part 1* pp 351–3
- Jensen J A and Munk P 1997 Computer phantoms for simulating ultrasound B-mode and CFM images *Acoustical Imaging* (Boston, MA: Springer) pp 75–80
- Jensen J A and Munk P 1998 A new method for estimation of velocity vectors *IEEE Trans. Ultrason. Ferroelectr. Freq. Control* **45** 837–51
- Jensen J A and Nikolov S I 2002 Transverse flow imaging using synthetic aperture directional beamforming *2002 IEEE Ultrasonics Symp., 2002. Proc. vol 2* pp 1523–7
- Jensen J A, Nikolov S, Yu A C H and Garcia D 2016a Ultrasound vector flow imaging: I: sequential systems *IEEE Trans. Ultrason. Ferroelectr. Freq. Control* **63** 1704–21
- Jensen J, Nikolov S, Yu A C H and Garcia D 2016b Ultrasound vector flow imaging: II: parallel systems *IEEE Trans. Ultrason. Ferroelectr. Freq. Control* **63** 1722–32
- Kerr A T and Hunt J W 1992a A method for computer simulation of ultrasound Doppler color flow images—I. Theory and numerical method *Ultrasound Med. Biol.* **18** 861–72
- Kerr A T and Hunt J W 1992b A method for computer simulation of ultrasound Doppler color flow images—II. Simulation results *Ultrasound Med. Biol.* **18** 873–9
- Li Y and Zagzebski J A 1999 A frequency domain model for generating B-mode images with array transducers *IEEE Trans. Ultrason. Ferroelectr. Freq. Control* **46** 690–9
- Liu M B and Liu G R 2010 Smoothed particle hydrodynamics (SPH): an overview and recent developments *Arch. Comput. Methods Eng.* **17** 25–76
- Madiena C, Faurie J, Porée J and Garcia D 2018 Color and vector flow imaging in parallel ultrasound with sub-Nyquist sampling *IEEE Trans. Ultrason. Ferroelectr. Freq. Control* **65** 795–802
- Mao W, Caballero A, McKay R, Primiano C and Sun W 2017 Fully-coupled fluid-structure interaction simulation of the aortic and mitral valves in a realistic 3D left ventricle model *PLoS One* **12** e0184729
- Mao W, Li K and Sun W 2016 Fluid-structure interaction study of transcatheter aortic valve dynamics using smoothed particle hydrodynamics *Cardiovasc. Eng. Technol.* **7** 374–88
- Mehregan F, Tournoux F, Muth S, Pibarot P, Rieu R, Cloutier G and Garcia D 2014 Doppler vortography: a color Doppler approach to quantification of intraventricular blood flow vortices *Ultrasound Med. Biol.* **40** 210–21
- Mo L Y L and Cobbold R S C 1986 A stochastic model of the backscattered Doppler ultrasound from blood *IEEE Trans. Biomed. Eng.* **BME-33** 20–7
- Monaghan J J 1992 Smoothed particle hydrodynamics *Annu. Rev. Astron. Astrophys.* **30** 543–74
- Monaghan J J 2012 Smoothed particle hydrodynamics and its diverse applications *Annu. Rev. Fluid Mech.* **44** 323–46
- Morris J P, Fox P J and Zhu Y 1997 Modeling low Reynolds number incompressible flows using SPH *J. Comput. Phys.* **136** 214–26
- Ovall J S 2016 The Laplacian and mean and extreme values *Am. Math. Mon.* **123** 287–91
- Papadofrangakis E, Engeler W E and Fakiris J A 1981 Measurement of true blood velocity by an ultrasound system US Patent 4,265,126 (<https://patents.google.com/patent/US4265126/en>)

- Pibarot P, Garcia D and Dumesnil J G 2013 Energy loss index in aortic stenosis. From fluid mechanics concept to clinical application *Circulation* **127** 1101–4
- Price D J 2012 Smoothed particle hydrodynamics and magnetohydrodynamics *J. Comput. Phys.* **231** 759–94
- Ricci S, Ramalli A, Bassi L, Boni E and Tortoli P 2018 Real-time blood velocity vector measurement over a 2D region *IEEE Trans. Ultrason. Ferroelectr. Freq. Control* **65** 201–9
- Schmerr L W Jr 2015a *Fundamentals of Ultrasonic Phased Arrays* (Berlin: Springer)
- Schmerr L W Jr 2015b Phased array beam modeling (1D elements) *Fundamentals of Ultrasonic Phased Arrays (Solid Mechanics and its Applications)* (Berlin: Springer) pp 73–98
- Selfridge A R, Kino G S and Khuri-Yakub B T 1980 A theory for the radiation pattern of a narrow-strip acoustic transducer *Appl. Phys. Lett.* **37** 35–6
- Shahriari S and Kadem L 2018 Smoothed particle hydrodynamics method and its applications to cardiovascular flow modeling *Numerical Methods and Advanced Simulation in Biomechanics and Biological Processes* (New York: Academic) pp 203–19
- Shahriari S, Hassan I G and Kadem L 2013 Modeling unsteady flow characteristics using smoothed particle hydrodynamics *Appl. Math. Model.* **37** 1431–50
- Shahriari S, Kadem L, Rogers B D and Hassan I 2012a Smoothed particle hydrodynamics method applied to pulsatile flow inside a rigid two-dimensional model of left heart cavity *Int. J. Numer. Methods Biomed. Eng.* **28** 1121–43
- Shahriari S, Maleki H, Hassan I and Kadem L 2012b Evaluation of shear stress accumulation on blood components in normal and dysfunctional bileaflet mechanical heart valves using smoothed particle hydrodynamics *J. Biomech.* **45** 2637–44
- Springel V 2010 Smoothed particle hydrodynamics in astrophysics *Annu. Rev. Astron. Astrophys.* **48** 391–430
- Stein J H, Korcarz C E, Hurst R T, Lonn E, Kendall C B, Mohler E R, Najjar S S, Rembold C M and Post W S 2008 Use of carotid ultrasound to identify subclinical vascular disease and evaluate cardiovascular disease risk: a consensus statement from the american society of echocardiography carotid intima-media thickness task force endorsed by the society for vascular medicine *J. Am. Soc. Echocardiogr.* **21** 93–111
- Stepanishen P R 1971 Transient radiation from pistons in an infinite planar baffle *J. Acoust. Soc. Am.* **49** 1629–38
- Swillens A, Degroote J, Vierendeels J, Lovstakken L and Segers P 2010 A simulation environment for validating ultrasonic blood flow and vessel wall imaging based on fluid-structure interaction simulations: ultrasonic assessment of arterial distension and wall shear rate *Med. Phys.* **37** 4318–30
- Swillens A, Lovstakken L, Kips J, Torp H and Segers P 2009 Ultrasound simulation of complex flow velocity fields based on computational fluid dynamics *IEEE Trans. Ultrason. Ferroelectr. Freq. Control* **56** 546–56
- Tanter M, Bercoff J, Sandrin L and Fink M 2002 Ultrafast compound imaging for 2D motion vector estimation: application to transient elastography *IEEE Trans. Ultrason. Ferroelectr. Freq. Control* **49** 1363–74
- Trahey G E, Allison J W and von Ramm O T 1987 Angle independent ultrasonic detection of blood flow *IEEE Trans. Biomed. Eng.* **BME-34** 965–7
- Treeby B E and Cox B T 2010 k-wave: MATLAB toolbox for the simulation and reconstruction of photoacoustic wave fields *J. Biomed. Opt.* **15** 021314
- Varray F, Basset O, Tortoli P and Cachard C 2013 CREANUIS: a non-linear radiofrequency ultrasound image simulator *Ultrasound Med. Biol.* **39** 1915–24
- Yamaguchi T, Ishikawa T, Imai Y, Matsuki N, Xenos M, Deng Y and Bluestein D 2010 Particle-based methods for multiscale modeling of blood flow in the circulation and in devices: challenges and future directions *Ann. Biomed. Eng.* **38** 1225–35
- Yiu B Y S, Lai S S M and Yu A C H 2014 Vector projectile imaging: time-resolved dynamic visualization of complex flow patterns *Ultrasound Med. Biol.* **40** 2295–309
- Zhao S Z, Papatheanasopoulou P, Long Q, Marshall I and Xu X Y 2003 Comparative study of magnetic resonance imaging and image-based computational fluid dynamics for quantification of pulsatile flow in a carotid bifurcation phantom *Ann. Biomed. Eng.* **31** 962–71
- Zhou Y, Giffard-Roisin S, Craene M D, Camarasu-Pop S, D'Hooge J, Alessandrini M, Friboulet D, Sermesant M and Bernard O 2018 A framework for the generation of realistic synthetic cardiac ultrasound and magnetic resonance imaging sequences from the same virtual patients *IEEE Trans. Med. Imaging* **37** 741–54